ABHINANDAN JAIN [*], *CALVIN KUO* [**], *PARAMSOTHY JAYAKUMAR* [***],
JONATHAN CAMERON [*]

CONSTRAINT EMBEDDING FOR VEHICLE SUSPENSION DYNAMICS

The goal of this research is to achieve close to real-time dynamics performance for allowing auto-pilot in-the-loop testing of unmanned ground vehicles (UGV) for urban as well as off-road scenarios. The overall vehicle dynamics performance is governed by the multibody dynamics model for the vehicle, the wheel/terrain interaction dynamics and the onboard control system. The topic of this paper is the development of computationally efficient and accurate dynamics model for ground vehicles with complex suspension dynamics. A challenge is that typical vehicle suspensions involve closed-chain loops which require expensive DAE integration techniques. In this paper, we illustrate the use the alternative constraint embedding technique to reduce the cost and improve the accuracy of the dynamics model for the vehicle.

1. Introduction

In this paper, we describe the constraint embedding approach for modeling the dynamics of a 4-wheeled HMMWV vehicle, that has a double wishbone suspension and an associated spring-damper unit at each wheel. Each of these wheel suspensions contains a number of articulated bodies with multiple kinematic closed loops. Despite the large number of internal degrees of freedom, due to the constraints, each suspension unit has only a single effective degree of freedom.

The standard approach for modeling closed-chain system dynamics [1] entails decomposing the system into a tree-topology system (or even a col-

---

[*] *Jet Propulsion Laboratory, California Institute of Technology, 4800 Oak Grove Drive, Pasadena, California 91016, USA; E-mail: jain@jpl.nasa.gov, jmc@jpl.nasa.gov*

[**] *Department of Mechanical Engineering, Stanford University, Palo Alto, California 91016, USA; E-mail: calvink@stanford.edu*

[***] *U.S. Army TARDEC, 6501 E 11 Mile Rd, Warren, MI 48397, USA; E-mail: paramsothy.jayakumar.civ@mail.mil*

lection of independent bodies) and appending the closed-chain bilateral constraints to the equations of motion. A drawback of this approach is the increased computation for solving the equations of motion. Another serious drawback is the error drift that arises during the integration of the multibody dynamics equations of motion. This error drift is usually handled by the use of a differential-algebraic equation (DAE) solver and error correction algorithms to manage the constraint error over time, adding even more computational cost and accuracy error to the dynamics solution. Our desire for real-time performance requires us to address these major computational drawbacks of the conventional approaches for closed-chain dynamics as a step towards attaining the real-time goal.

The recently developed *constrained embedding (CE)* method [2, 3] overcomes these drawbacks for closed-chain dynamics models. In this paper we describe the application of the constraint embedding approach for the vehicle and suspension dynamics. The constraint embedded technique converts all constraint loops into compound bodies with variable configuration that have the same number of degrees of freedom as the number of independent degrees of freedom for the loops they replace. These compound bodies internally handle their internal degrees of freedom and constraints, effectively hiding them from the dynamics solver. The resulting system topology is once again a tree with only inter-body hinges and no bilateral constraints. The benefit of this approach is that structure-based $O(\mathcal{N})$ tree algorithms can be directly used to solve the dynamics, and this formulation results in an ODE instead of a DAE. Thus extra error control techniques are not needed. This method however is more complex to implement, since the aggregated bodies now have configuration dependent geometry. While CE method shares the minimal coordinates attribute with projection dynamics techniques [1, 4], its advantage lies in the preservation of the system's tree topology that is necessary for the use of the low-cost structure-based tree algorithms.

In this paper we describe the CE modeling approach for the individual wheel suspensions, the overall vehicle dynamics model, and the adaptation of the recursive $O(\mathcal{N})$ dynamics algorithm for efficiently solving the equations of motion. While generic iterative methods can be used to solve the kinematics for the loops, we also describe analytical techniques that significantly improve performance speed up and accuracy. In this paper we focus only on vehicle dynamics. See references ([5] and [6] papers) for terramechanics and closed-loop shared control scenario modeling using this approach.

We begin in Section 2 with an overview of the $O(\mathcal{N})$ ODE techniques for solving the dynamics of a tree-topology dynamics system. Section 3 takes up the dynamics of non-tree topology systems, i.e. systems with closed-loop constraints that is typical of vehicle suspension systems. We provide an overview

of the constraint embedding technique that solves closed-chain dynamics using $O(\mathcal{N})$ ODE techniques, and describe the key differences in handling aggregated bodies. Section 4 describes the HMMWV vehicle and the dynamics model including the CE model for its double-wishbone wheel suspensions. Finally, in Section 5 we describe analytical techniques that can be used for the double-wishbone suspension kinematics to further speed up the dynamics computations and improve their accuracy. The research described in this paper was presented at a recent conference on mutibody dynamics [7].

2. Recursive tree system dynamics

The equations of motion for a multibody system with tree topology (i.e. no closed loop constraints) and a $\mathcal{N}$ degrees of freedom are of the form

$$\mathcal{T} = \mathcal{M}(\theta)\ddot{\theta} + \mathcal{C}(\theta, \dot{\theta}) \tag{1}$$

Here $\mathcal{M} \in \mathcal{R}^{\mathcal{N} \times \mathcal{N}}$ denotes the mass matrix for the serial-chain system, and $\mathcal{C} \in \mathcal{R}^{\mathcal{N}}$ is the vector of velocity dependent nonlinear Coriolis and velocity dependent terms, and gravitational and external forces. The $\mathcal{N}$ dimensional stacked vectors θ, $\dot{\theta}$ and $\mathcal{T}$ denote the system generalized coordinates, generalized velocities and generalized forces. In this form, the tree-topology equations of motion can be propagated using an ODE integrator.

Using spatial operator techniques [3, 8], the following Newton-Euler Factorization expression for the mass matrix in Eq. 1 and $\mathcal{C}$ can be obtained:

$$\mathcal{M}(\theta) = H\phi M\phi^*H^* \in \mathcal{R}^{\mathcal{N} \times \mathcal{N}} \quad \text{and} \quad \mathcal{C}(\theta, \dot{\theta}) \stackrel{\triangle}{=} H\phi(M\phi^*\mathfrak{a} + \mathfrak{b}) \in \mathcal{R}^{\mathcal{N}} \tag{2}$$

With $\mathfrak{n}$ denoting the number of bodies in the system, the $H \in \mathcal{R}^{\mathcal{N} \times 6\mathfrak{n}}$ and $M \in \mathcal{R}^{6\mathfrak{n} \times 6\mathfrak{n}}$ spatial operators are block diagonal with the hinge axes and body spatial inertia matrices for each of the bodies being the diagonal elements respectively. The block lower-triangular $\phi \in \mathcal{R}^{6\mathfrak{n} \times 6\mathfrak{n}}$ operator's elements are the 6×6 rigid body transformation matrices for body pairs in the system. The $\mathfrak{a}$ stacked vector contains the the body Coriolis accelerations, while $\mathfrak{b}$ contains the body gyroscopic, external and gravitational forces for the system.

Further use of spatial operator techniques [3,8] can be used to obtain the following analytical *innovations* factorization and inversion expressions for the mass matrix:

$$\mathcal{M} = H\phi M\phi^* H^*$$
$$\mathcal{M} = [I + H\phi\mathcal{K}]\,\mathcal{D}\,[I + H\phi\mathcal{K}]^*$$
$$[I + H\phi\mathcal{K}]^{-1} = [I - H\psi\mathcal{K}]$$
$$\mathcal{M}^{-1} = [I - H\psi\mathcal{K}]^*\,\mathcal{D}^{-1}\,[I - H\psi\mathcal{K}] \tag{3}$$

The component elements of the ψ, $\mathcal{D}$, and $\mathcal{K}$ spatial operators are obtained from the following tip-to-base *articulated body (AB)* Riccati equation recursion described here for the kth body:

$$\mathcal{P}^+(c) = \overline{\tau}(c)\mathcal{P}(c)$$
$$\mathcal{P}(k) = \sum_{\forall c \in \mathbb{C}(k)} \phi(k,c)\mathcal{P}^+(c)\phi^*(k,c) + M(k)$$
$$\mathcal{D}(k) = H(k)\mathcal{P}(k)H^*(k) \tag{4}$$
$$\mathcal{G}(k) = \mathcal{P}(k)H^*(k)\mathcal{D}^{-1}(k)$$
$$\tau(k) = \mathcal{G}(k)H(k)$$

In the above, $\mathbb{C}(k)$ denotes the set of bodies that are the immediate children of the kth body.

The analytical expression for $\mathcal{M}^{-1}$ in Eq. 3 allows to explicitly solve Eq. 1 and develop the following expression for the generalized accelerations:

$$\ddot{\theta} = [I - H\psi\mathcal{K}]^*\,\mathcal{D}^{-1}\big[\mathcal{T} - H\psi(\mathcal{K}\mathcal{T} + \mathcal{P}\mathfrak{a} + \mathfrak{b})\big] - \mathcal{K}^*\psi^*\mathfrak{a} \tag{5}$$

Eq. 5 can be converted into the $O(\mathcal{N})$ AB recursive forward dynamics algorithm. The tip-to-base gather recursion steps for the kth body has the following form:

$$\mathfrak{z}^+(c) = \mathfrak{z}(c) + \mathcal{G}(c)\epsilon(c)$$
$$\mathfrak{z}(k) = \sum_{\forall c \in \mathbb{C}(k)} \phi(k,c)\mathfrak{z}^+(c) + \mathfrak{b}(k) + \mathcal{P}(k)\mathfrak{a}(k)$$
$$\epsilon(k) = \mathcal{T}(k) - H(k)\mathfrak{z}(k)$$
$$\nu(k) = \mathcal{D}^{-1}(k)\epsilon(k) \tag{6}$$

The base-to-tip steps from body p to it's child body k are as follows:

$$\alpha^+(k) = \phi^*(p,k)\alpha(p)$$
$$\ddot{\theta}(k) = \nu(k) - \mathcal{G}^*(k)\alpha^+(k) \tag{7}$$
$$\alpha(k) = \alpha^+(k) + H^*(k)\ddot{\theta}(k) + \mathfrak{a}(k)$$

The AB algorithm is the lowest order algorithm available for solving the forward dynamics of tree-topology systems.

3. Closed chain dynamics

Multibody systems with closed-loop constraints can be decomposed into an tree-topology system subject to explicit bilateral constraints. The decomposition is not unique. A common option is to define the tree-topology system as consisting of all the component bodies as independent bodies with the set of constraints containing all the loop constraints as well as constraints for all the inter-body hinges as shown in Fig. 1a. In this *fully-augmented (FA)* approach the dynamics model and constraints dimension is large but with sparse structure. In the alternative *tree-augmented (TA)* approach, the tree-topology system is chosen such that the number of explicit constraints is the minimum
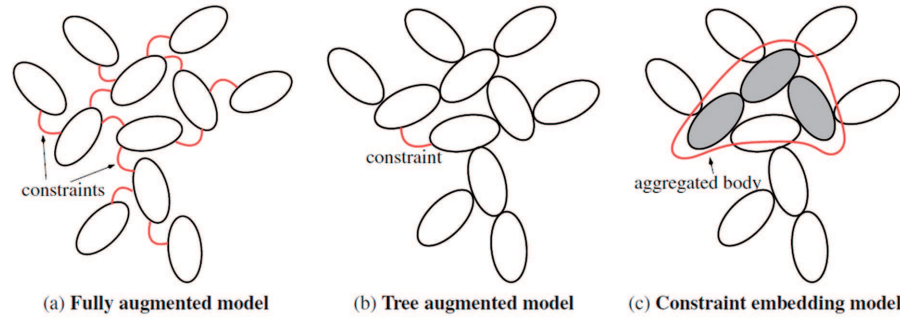

(a) **Fully augmented model** (b) **Tree augmented model** (c) **Constraint embedding model**

Fig. 1. In the fully augmented model (a), all bodies are treated as independent bodies with inter--body constraints. In the tree augmented model (b), the system is decomposed into a tree system together with a minimal set of inter-body constraints. In the constraint embedding model (c), internal loops are aggregated into bodies to convert the system into a tree topology system

number as illustrated in Fig. 1b. The size of the dynamics model is much smaller, but the mass matrix has much less sparsity. In either case, the equations of motion for multibody systems with closed-loop constraints have the following form:

$$\begin{pmatrix} \mathcal{M} & G_c^* \\ G_c & 0 \end{pmatrix} \begin{bmatrix} \ddot{\theta} \\ -\lambda \end{bmatrix} = \begin{bmatrix} \mathcal{T} - \mathcal{C} \\ \acute{\mathcal{U}} \end{bmatrix} \quad \text{where} \quad \acute{\mathcal{U}} \triangleq \dot{\mathcal{U}}(t) - \dot{G}_c \dot{\theta} \in \mathcal{R}^{n_c}$$

(8)

Here G_c denotes the constraint matrix, and λ the Lagrange multipliers corresponding to the constraints. DAE integration techniques are required for solving the Eq. 8 dynamics model. One approach to solving the closed-chain dynamics equations of motion is to assemble the matrix on the left and the vector on the right in Eq. 8 and solve the linear matrix equation for the $\ddot{\theta}$

generalized accelerations. This is especially attractive for the FA model, since the $\mathcal{M}$ matrix for this case is block diagonal and constant. Indeed, the whole matrix is highly sparse for this case. This approach is analyzed in detail in reference [4]. In the TA approach, the $O(\mathcal{N})$ AB algorithm can be used for the tree-topology component and is described in reference [9].

3.1. Constraint Embedding Approach

At the heart of the constraint embedding strategy for closed-chain systems is the transformation of a non-tree topology system into a tree topology system. The approach is to isolate non-tree sub-graphs and remove them using aggregation to transform the system digraph into a tree. The constraint embedding transformation is illustrated illustrated in Fig. 1c. The constraint embedding strategy involves the following steps:

1. Decompose the non-tree digraph for the system into a spanning tree, $\mathfrak{T}$, and a collection of cut-edges for the constraints. The set of cut-edges is usually not unique.
2. For each cut-edge, identify the aggregation sub-graph, $\mathfrak{S}$, for the sub-graph consisting of the node pair for the cut-edge.
   A procedure for creating this $\mathfrak{S}$ aggregation sub-graph is is as follows:
   (a) Identify the smallest sub-tree that contains the nodes in the cut-edge.
   (b) Remove the root node from this sub-tree to obtain the aggregation sub-graph $\mathfrak{S}$ for the aggregated body.

At the conclusion of the constrained embedding process, all of the constraints are absorbed into the aggregated links. As a result, we once again have a tree-topology system and the mass matrix factorization and inversion results, as well as the $O(\mathcal{N})$ AB algorithm for solving the dynamics as described in Section 2 can be extended and applied to the closed-chain system as discussed in detail in [2, 3].

3.2. Recursive CE Forward Dynamics

In this section we focus on the differences in the AB recursive dynamics procedure that are specific to the aggregated body $\mathfrak{S}$. Towards this, let $S(\mathfrak{S})$ denote the set of articulated rigid bodies contained within the $\mathfrak{S}$ body, $n(\mathfrak{S})$ the number of these bodies, $\mathcal{N}_f(\mathfrak{S})$ the number of generalized velocities associated with all the bodies in $S(\mathfrak{S})$, and $\mathcal{N}(\mathfrak{S})$ the number of independent generalized velocities for the $\mathfrak{S}$ body. The $\dot{\theta}(\mathfrak{S})$ generalized velocities for the $\mathfrak{S}$ body are the $\mathcal{N}(\mathfrak{S})$ independent generalized velocities among the sum total of $\mathcal{N}_f(\mathfrak{S})$ generalized velocities $\underline{\dot{\theta}}_{\mathfrak{S}}$ for the individual rigid bodies within $S(\mathfrak{S})$. Let $X_{\mathfrak{S}} \in \mathcal{R}^{\mathcal{N}_f(\mathfrak{S}) \times \mathcal{N}(\mathfrak{S})}$ denote the configuration dependent matrix

that maps the $\dot{\theta}(\mathfrak{S})$ independent generalized velocities into the $\underline{\dot{\theta}}_{\mathfrak{S}}$ set of internal generalized velocities such that

$$\underline{\dot{\theta}}_{\mathfrak{S}} \triangleq \begin{bmatrix} \dot{\theta}(j_1) \\ \vdots \\ \dot{\theta}(j_{n(\mathfrak{S})}) \end{bmatrix} = X_{\mathfrak{S}} \dot{\theta}(\mathfrak{S}) \quad \text{and} \quad \mathcal{T}(\mathfrak{S}) = X_{\mathfrak{S}}^* \begin{bmatrix} \mathcal{T}(j_1) \\ \vdots \\ \mathcal{T}(j_{n(\mathfrak{S})}) \end{bmatrix} \quad (9)$$
$$\text{where} \quad j_i \in S(\mathfrak{S})$$

Also, for the aggregated body

$$M(\mathfrak{S}) \triangleq \text{diag}\left\{M(i)\right\}_{i \in S(\mathfrak{S})} \in \mathcal{R}^{6n(\mathfrak{S}) \times 6n(\mathfrak{S})}$$

$$H(\mathfrak{S}) \triangleq X_{\mathfrak{S}}^* \underline{H}_{\mathfrak{S}} \in \mathcal{R}^{\mathcal{N}(\mathfrak{S}) \times 6n(\mathfrak{S})}$$

$$\text{where} \quad \underline{H}_{\mathfrak{S}} \triangleq \text{diag}\left\{H(i)\right\}_{i \in S(\mathfrak{S})} \in \mathcal{R}^{\mathcal{N}_f(\mathfrak{S}) \times 6n(\mathfrak{S})}$$

$$\phi(\mathfrak{S}, c) \triangleq \begin{bmatrix} 0 \\ \vdots \\ \phi(\wp(c)) \\ \vdots \\ 0 \end{bmatrix} \in \mathcal{R}^{6n(\mathfrak{S}) \times 6} \quad \text{where} \quad \wp(c) \in S(\mathfrak{S})$$

$$\phi(p, \mathfrak{S}) \triangleq [\phi(p, j_1), \cdots, \phi(p, j_{n(\mathfrak{S})})] \in \mathcal{R}^{6 \times 6n(\mathfrak{S})} \quad \text{where} \quad j_i \in S(\mathfrak{S})$$
(10)

$\wp(c)$ denotes parent body for the c body, and p is the parent body for the aggregated body. One noticeable difference is that the quantities associated with the $\mathfrak{S}$ aggregated body have row/column dimension $6n(\mathfrak{S})$ instead of just 6 encountered for regular rigid bodies. For the vectorial quantities we have

$$\mathfrak{b}(\mathfrak{S}) \triangleq \begin{bmatrix} \mathfrak{b}(j_1) \\ \vdots \\ \mathfrak{b}(j_{n(\mathfrak{S})}) \end{bmatrix} \in \mathcal{R}^{6n(\mathfrak{S})} \quad \text{and} \quad \mathfrak{a}(\mathfrak{S}) \triangleq \begin{bmatrix} \mathfrak{a}(j_1) \\ \vdots \\ \mathfrak{a}(j_{n(\mathfrak{S})}) \end{bmatrix} + \quad (11)$$
$$+\underline{H}_{\mathfrak{S}}^* \dot{X}_{\mathfrak{S}} \dot{\theta} \in \mathcal{R}^{6n(\mathfrak{S})} \quad \text{where} \quad j_i \in S(\mathfrak{S})$$

Though the dimensions are larger, we can also see that many of these quantities have highly sparse structure that can be used to reduce the cost of the steps in the AB forward dynamics recursions. The most computationally expensive

part of the AB steps is the computation and inversion of the $\mathcal{D}(\mathfrak{S})$ symmetric, positive definite matrix in Eq. 4. Its size is the number of independent degrees of freedom for the aggregated link. Thus, the computational cost of the AB algorithm is no longer linear in the number of independent degrees of freedom for the aggregated links, but, instead, is (in the worst case) quadratic in the total degrees of freedom in the $\mathfrak{S}$ aggregation sub-graph, and cubic in the number of independent degrees of freedom in the $\mathfrak{S}$ sub-graph. These additional costs, however, are modest when the loops are of moderate size.

3.3. CE Kinematics

The CE dynamics solution process also requires the following kinematics computations:

1. forward kinematics computation that maps the independent $\theta(\mathfrak{S})$ coordinates into the $\underline{\theta}_{\mathfrak{S}}$ full generalized coordinates values for the $\mathfrak{S}$ CE graph.
2. velocity kinematics computation of the $X_{\mathfrak{S}}$ matrix in Eq. 9 that maps the $\dot{\theta}(\mathfrak{S})$ independent generalized velocities into the $\underline{\dot{\theta}}_{\mathfrak{S}}$ internal generalized velocities for the $\mathfrak{S}$.
3. the $\dot{X}_{\mathfrak{S}}\dot{\theta}(\mathfrak{S})$ vector needed in Eq. 11.

In this section we describe the general numerical procedures for carrying out the kinematics computations in the above steps, before exploring analytical techniques for the HMMWV suspension in Section 3.3 that are both faster and more accurate. The general method for carrying out the forward kinematics computation in step (1) is to use a Newton-like iterative procedure to converge on the solution that satisfies the constraints within the $\mathfrak{S}$ subgraph.

We now derive the general expression for the configuration dependent $X_{\mathfrak{S}}$ matrix for step (2). For loop constraints, we have an algebraic constraint on the relative velocities of a pair of physical closure nodes in the sub-graph. Denoting a representative pair of closure nodes as o and p, such a constraint can be expressed as

$$\delta_{\mathfrak{S}} = A(\mathcal{V}_o - \mathcal{V}_p) = A(\mathcal{J}_o - \mathcal{J}_p)\underline{\dot{\theta}}_{\mathfrak{S}} = Y\underline{\dot{\theta}}_{\mathfrak{S}} = [Y_1, \ Y_2] \begin{bmatrix} \underline{\dot{\theta}}_{u\mathfrak{S}} \\ \dot{\theta}(\mathfrak{S}) \end{bmatrix} \quad (12)$$

Here, A denotes the constraint on the relative spatial velocities between this pair of closure nodes, and $\mathcal{J}_o$, $\mathcal{J}_p$ denote sub-graph Jacobians relating the generalized velocities of the sub-graph to the spatial velocities at the o and p closure nodes. Also, $Y \stackrel{\triangle}{=} A(\mathcal{J}_o - \mathcal{J}_p)$, $\underline{\dot{\theta}}_{u\mathfrak{S}}$ is the complement of the $\dot{\theta}(\mathfrak{S})$ sub-vector in $\underline{\dot{\theta}}_{\mathfrak{S}}$ and represents the dependent generalized velocity coordinates. $\mathcal{J}_{o1}$, etc., and Y_1 and Y_2 represent sub-blocks within Y. When the $\underline{\dot{\theta}}_{\mathfrak{S}}$

generalized velocities satisfy the constraints within $\mathfrak{S}$, the constraint velocity error $\delta_\mathfrak{S} = 0$. With partitioning chosen such that Y_1 is square and full rank it follows from Eq. 12 that:

$$\dot{\underline{\theta}}_{u\mathfrak{S}} = -Y_1^{-1}Y_2\,\dot{\theta}(\mathfrak{S}) \quad \Longrightarrow \quad X_\mathfrak{S} = \begin{bmatrix} -Y_1^{-1}Y_2 \\ I \end{bmatrix} \tag{13}$$

The following derives an expression for $\dot{X}_\mathfrak{S}\dot{\theta}(\mathfrak{S})$ needed in step (3). With $Z \triangleq Y_1^{-1}Y_2$, we have

$$\frac{dZ}{dt} = \frac{dY_1^{-1}}{dt}Y_2 + Y_1^{-1}\frac{dY_2}{dt} = -Y_1^{-1}\frac{dY_1}{dt}Y_1^{-1}Y_2 + Y_1^{-1}\frac{dY_2}{dt} = Y_1^{-1}\left[\frac{dY_2}{dt} - \frac{dY_1}{dt}Z\right]$$

Thus,

$$\dot{X}_\mathfrak{S} = \begin{bmatrix} -\dot{Z} \\ 0 \end{bmatrix} = \begin{bmatrix} Y_1^{-1}\left[\dot{Y}_1 Z - \dot{Y}_2\right] \\ 0 \end{bmatrix} = \begin{bmatrix} -Y_1^{-1}\dot{Y}X_\mathfrak{S} \\ 0 \end{bmatrix} \Longrightarrow \dot{X}_\mathfrak{S}\dot{\theta}(\mathfrak{S}) = \begin{bmatrix} -Y_1^{-1}\dot{Y}\dot{\underline{\theta}}_\mathfrak{S} \\ 0 \end{bmatrix}$$

Now from Eq. 12 it follows that

$$\dot{\delta}_\mathfrak{S} = \dot{Y}\dot{\underline{\theta}}_\mathfrak{S} + Y\ddot{\underline{\theta}}_\mathfrak{S} \Longrightarrow \dot{Y}\dot{\underline{\theta}}_\mathfrak{S} = \left[\dot{\delta}_\mathfrak{S}\right]_{\ddot{\underline{\theta}}_\mathfrak{S}=0} \Longrightarrow \dot{X}_\mathfrak{S}\dot{\theta}(\mathfrak{S}) = \begin{bmatrix} -Y_1^{-1}\left[\dot{\delta}_\mathfrak{S}\right]_{\ddot{\underline{\theta}}_\mathfrak{S}=0} \\ 0 \end{bmatrix}$$

$$\tag{14}$$

Note that while $\delta_\mathfrak{S}$ represents the velocity level constraint violation error within $\mathfrak{S}$, $\dot{\delta}_\mathfrak{S}$ represents the acceleration level constraint violation error. These quantities are easily computed using the normal kinematics procedures for given $\dot{\underline{\theta}}_\mathfrak{S}$ and $\ddot{\underline{\theta}}_\mathfrak{S}$ values. $\left[\dot{\delta}_\mathfrak{S}\right]_{\ddot{\underline{\theta}}_\mathfrak{S}=0}$ represents the acceleration level error with $\ddot{\underline{\theta}}_\mathfrak{S} = 0$, i.e. just the velocity dependent contribution to the acceleration level error. Eq. 13 and Eq. 14 together provide general solutions for computing $X_\mathfrak{S}$ and $\dot{X}_\mathfrak{S}\dot{\theta}(\mathfrak{S})$ needed for solving the CE dynamics.

4. The HMMWV Vehicle

The HMMWV vehicle has four independently suspended wheels and a steering linkage controlling the front wheel pair as shown in Fig. 2. The HMMWV employs a double wishbone suspension for all of its wheels that offer more robustness than the similar McPherson strut and less complexity than the multi-link suspension. Each of the wheel suspensions are connected to the vehicle chassis via bushings. Including the compliance of the bushings in the dynamics model leads to a tree topology model for the vehicle

and its suspensions, and thus the efficient $O(\mathcal{N})$ AB dynamics algorithm and the ODE formulation from Section 2 can be directly applied for solving the vehicle's equations of motion. An alternative modeling option described in [10] for allowing larger integrator time steps is to treat the bushings as being infinitely stiff – and hence as forming bilateral constraints between the suspensions and the chassis. In this case, the vehicle dynamics topology with the double wishbone suspension and the steering linkage contains closed loops. Due to these loops, the vehicle model topology no longer has a tree topology, and the $O(\mathcal{N})$ AB algorithm and ODE formulation for tree systems can no longer be used. In the rest of this paper we describe the use of the constraint embedding technique for recovering the use of the $O(\mathcal{N})$ AB algorithms and ODE formulation for this more challenging vehicle dynamics model.
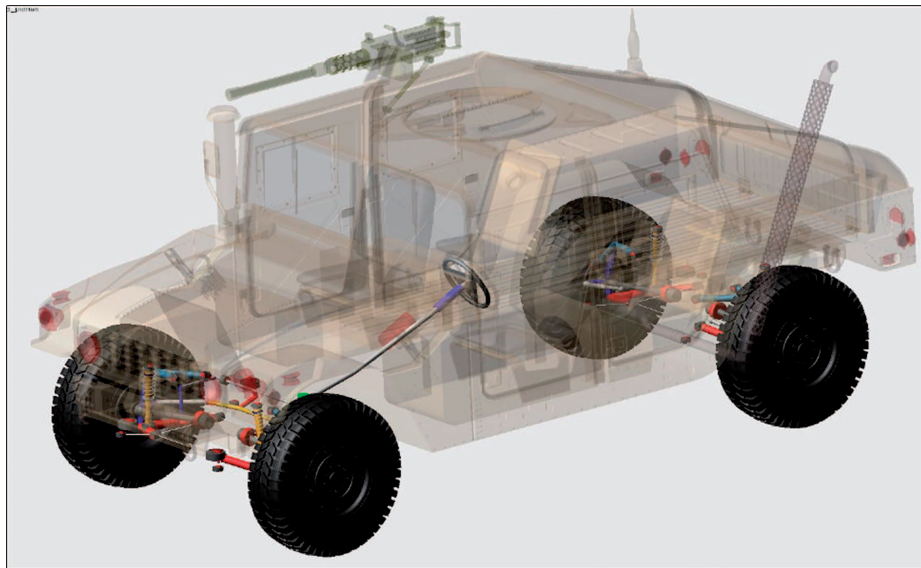

Fig. 2. The HMMWV vehicle with the double wishbone wheel suspensions from reference [11]

The double wishbone suspension (Fig. 3) is comprised of two control arms that form a fourbar linkage with the spindle and the HMMWV chassis. In addition, the lower control arm forms a slider-crank linkage with the shock absorber and the HMMWV chassis. Finally, there is a tie-rod that connects to the spindle forming the final closed chain in the suspension. The spindle loop is unique in that it falls outside the plane of the other two loops and its main purpose is to control the steering angle of the wheels, which are connected to the spindle. In the front suspensions, the tie rod is attached to the steering bar while in the rear suspensions, the tie rod is attached to the HMMWV chassis, which fixes the steering angle of the rear wheels.
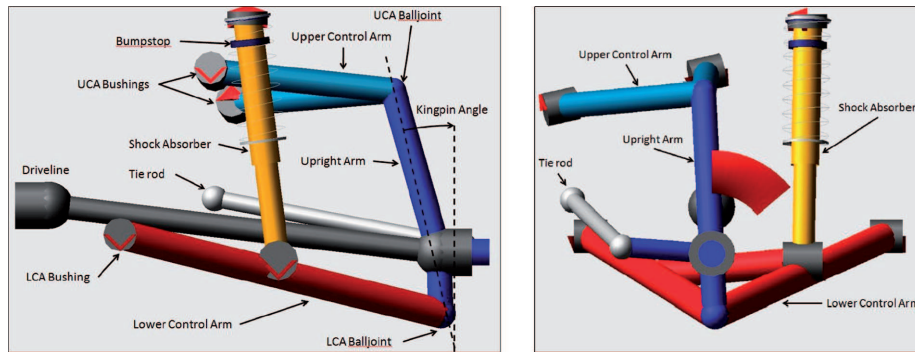
Fig. 3. The front and left views of the front wheel suspension from reference [11]

The joints that connect the two control arms with the spindle in the physical suspension are ball and socket joints and have full rotational degrees of freedom. This is useful for the physical suspension in which design imperfections and sudden shocks can bring the control arm loop out of plane. In the absence of such non-idealities, it is more efficient to represent these joints with a universal joint with one rotational degree of freedom along the spindle axis and the other in plane with the control arm loop. The joints that connects the tie rod to the spindle is also manufactured as a ball and socket joint in the physical HMMWV, however this introduces an uncontrolled rotational degree of freedom in the model in which the tie rod can freely spin about its own axis. Again, the joint connecting the tie rod and spindle can be modeled more simply as a universal joint.
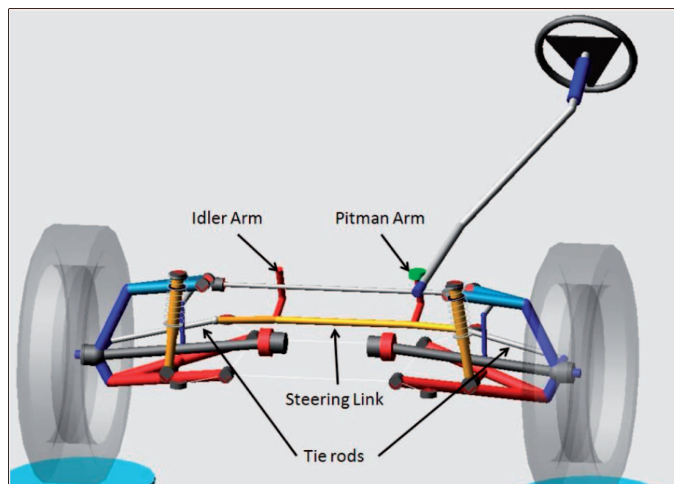

Fig. 4. The HMMWV vehicle with the front suspensions and the steering elements from reference [11]

The steering mechanism consists of a simple fourbar linkage (Fig. 4) comprised of the steering link, the pitman arm, the idler arm, and the HMMWV chassis. In our model, the steering is controlled by assigning a prescribed motion to the pitman arm. The ends of the steering arm are connected to the two front suspension tie rods and the resulting motion in the steering arm turns the front wheels about their spindle axes.

4.1. CE Model for the HMMWV Vehicle

A schematic for the double wishbone linkage for kinematic analysis is shown in Fig. 5. In the figure, AD is the lower control arm, DF the upright arm, FG the upper control arm. BI is the lower shock absorber arm, HJ the upper shock arm and HI the compression. EK denotes the spindle arm, and KL the tierod. The point L denotes the end of the tierod. For the rear wheels, L is attached to the vehicle chassis via a ball joint and its position is therefore fixed. For the pair of front wheels, the L points are attached to points on the steering arm that is a part of the Pitman steering mechanism as shown in Fig. 6. Steering is accomplished by changing the steering angle, which causes the steering arm to move the tierods and change the wheel orientations.
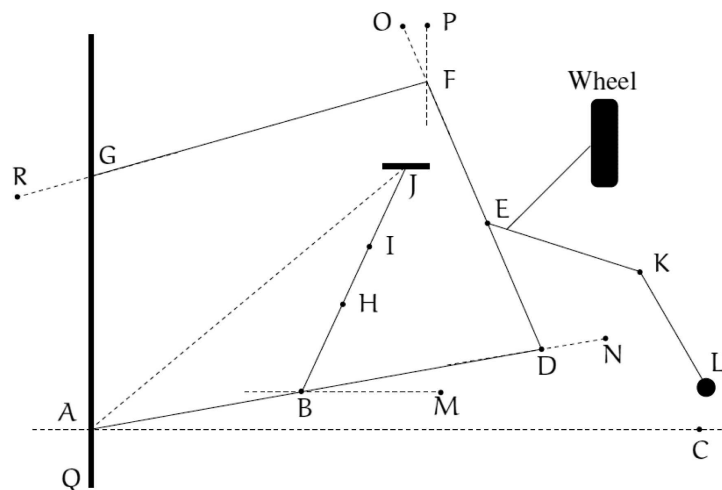
Fig. 5. Schematic for the double wishbone suspension assembly

Each wheel suspension has seven bodies (without including the wheel) and three constraints resulting in a single degree of freedom for each suspension. Each suspension is decomposed into a tree-topology system with the hinges at J, G and L being treated as constraints. Constraint embedding is used to model each suspension system as a individual single degree of freedom aggregated body. Each such aggregated body is attached to the chassis

parent body and in turn has a single wheel as a child body. The tierod end point locations for the front wheel suspensions are attached to the Pitman steering mechanism's steering link and are movable. While in principle the steering mechanism introduces additional constraints between the front wheel suspensions, for the purposes of this model we treat the steering mechanism kinematically so that its effect on the dynamics is only to set the position of the tierod end points as a function of the steering wheel angle. Thus the CE dynamics model consists of the chassis body, four suspension aggregated bodies and four wheel bodies with overall fourteen degrees of freedom. The CE $O(\mathcal{N})$ method described in Section 3 can be used to solve the equations of motion of this ODE model to simulate the vehicle dynamics.

5. Analytical double wishbone kinematics

Section 3.3 describes a numerical approach for computing the $X_{\mathbb{G}}$ needed for the constraint embedding dynamics. While the method is general, replacing it with analytical methods when possible provides a way to improve computational speed and accuracy.

In this section we derive analytical expressions for the forward kinematics, as well as the velocity level $X_{\mathbb{G}}$ for planar four-bar linkages, which will provide a stepping stone for developing expressions for the full HMMWV wheel suspensions. Each suspension has only a single degree of freedom, and we choose the generalized coordinate with the lower control arm, $\angle QAD$, as the independent generalized coordinate and denote it by the symbol θ.

The three loops in the suspension system are:

1. the ADFG *lower/upper control arm loop* consisting of the planar four-bar linkage containing the upper and lower control arms;
2. the ABJ *shock absorber loop* involving the planar shock absorber mechanism;
3. the EKL *spindle loop* involves the non-planar spindle and tie-rod mechanism.

We now derive analytical expressions for the forward kinematics as well as the velocity kinematics for each of the loops.

5.1. Lower/Upper control arm kinematics

For the forward kinematics we need to determine the values of all the dependent angles for a value of the independent angle. We do the initial derivation using absolute angles and use this to obtain expressions for the relative angle generalized coordinates. We use the following symbols for the four-bar parameters for the derivations within this section:

$$a = |GA|, \quad b = |AD|, \quad c = |DF|, \quad d = |FG|$$
$$\theta_3 = \angle PFO, \quad \theta_4 = \angle QGF$$

The forward kinematics problem for the lower/upper control arm loop is to determine the dependent generalized coordinates $\angle NDO$, $\angle OFG$ and $\angle RGA$ as functions of the $\theta = \angle QAD$ independent coordinate.

For 2D kinematic analysis, we use a derivation based on complex numbers and the 2D exponential $\exp(x) = \cos(x) + i\sin(x)$. We have

$$a + b\exp(i\theta) = c\exp(i\theta_3) + d\exp(i\theta_4) \tag{15}$$

Equating the real and imaginary parts leads to

$$a + b\cos(\theta) = c\cos(\theta_3) + d\cos(\theta_4)$$
$$b\sin(\theta) = c\sin(\theta_3) + d\sin(\theta_4) \tag{16}$$

Thus

$$c\cos(\theta_3) = a + b\cos(\theta) - d\cos(\theta_4) = x - d\cos(\theta_4)$$
$$\text{where} \quad x \triangleq a + b\cos(\theta)$$
$$c\sin(\theta_3) = b\sin(\theta) - d\sin(\theta_4) = y - d\sin(\theta_4) \tag{17}$$
$$\text{where} \quad y \triangleq b\sin(\theta)$$

Summing up the squares of both sides leads to

$$c^2 = x^2 + y^2 + d^2 - 2d(x\cos(\theta_4) + y\sin(\theta_4))$$
$$\Rightarrow \quad x\cos(\theta_4) + y\sin(\theta_4) = \frac{x^2 + y^2 + d^2 - c^2}{2d} \tag{18}$$

Dividing both sides by $\sqrt{x^2 + y^2}$ leads to

$$\cos(\theta_4 - \gamma) = \frac{x^2 + y^2 + d^2 - c^2}{2d\sqrt{x^2 + y^2}} \quad \text{where} \quad \gamma \triangleq \tan^{-1}\left(\frac{y}{x}\right) \tag{19}$$

Thus

$$\theta_4 = \gamma \pm \cos^{-1}\left(\frac{x^2 + y^2 + d^2 - c^2}{2d\sqrt{x^2 + y^2}}\right) \tag{20}$$

Note that we have two possible solutions for θ_4. Then from Eq. 17

$$\theta_3 = \tan^{-1}\left(\frac{y - d\sin(\theta_4)}{x - d\cos(\theta_4)}\right) \tag{21}$$

With the solution for the absolute angles, the values of the dependent generalized coordinates are

$$\angle NDO = \pi - (\theta - \theta_3), \ \angle OFG = \theta_4 - \theta_3 \ \text{ and } \ \angle RGA = \pi - \theta_4 \quad (22)$$

The above provide the analytical forward kinematics expressions for the lower/upper control arm four-bar linkage. For the velocity level expressions, it follows from Eq. 22 that

$$\angle \dot{N}DO = -(\dot{\theta} - \dot{\theta}_3), \quad \angle \dot{O}FG = \dot{\theta}_4 - \dot{\theta}_3 \quad \text{and} \quad \angle \dot{R}GA = -\dot{\theta}_4 \quad (23)$$

We thus need to determine analytical expressions for $\dot{\theta}_3$ and $\dot{\theta}_4$ relationships that map the independent. We begin by taking the time derivative of Eq. 15 to obtain

$$\dot{\theta}b \exp(i\theta) = \dot{\theta}_3 c \exp(i\theta_3) + \dot{\theta}_4 d \exp(i\theta_4)$$
$$\Rightarrow \quad \dot{\theta}b \exp(i(\theta - \theta_4)) = \dot{\theta}_3 c \exp(i(\theta_3 - \theta_4)) + \dot{\theta}_4 d \quad (24)$$

Equating the imaginary sides of both sides leads to

$$\dot{\theta}b \sin(\theta - \theta_4) = \dot{\theta}_3 c \sin(\theta_3 - \theta_4)$$
$$\Rightarrow \quad \dot{\theta}_3 = p\dot{\theta} \quad \text{where} \quad p \triangleq \frac{b \sin(\theta - \theta_4)}{c \sin(\theta_3 - \theta_4)} \quad (25)$$

Similarly

$$\dot{\theta}_4 = q\dot{\theta} \quad \text{where} \quad q \triangleq \frac{b \sin(\theta - \theta_3)}{d \sin(\theta_4 - \theta_3)} \quad (26)$$

This leads to the following closed-form expression for the four-bar portion of the $X_{\mathfrak{G}}$:

$$X_{\mathfrak{G}} = \begin{bmatrix} p - 1 \\ q - p \\ -q \end{bmatrix} \quad (27)$$

These equations represent a complete set of analytical kinematic expressions needed for constraint embedding solution process for a four-bar linkage.

5.2. Shock absorber loop kinematics

We use the following symbols for the shock absorber loop parameters within this section:

$$x = |AJ|, \quad y = |AB|, \quad z = |BJ|$$
$$\beta = \angle CQJ, \quad \eta = \angle CQB, \quad \gamma = \angle MBJ$$

The forward kinematics problem here is to determine the dependent generalized coordinates $\angle DBJ$ and the signed magnitude r of HI as functions of the θ independent coordinate. The assumption is that H and I coincide when the shock absorber compression is zero. We have

$$x \exp(i\beta) = y \exp(i\eta) + z \exp(i\gamma)$$
$$\Rightarrow \quad z \exp(i\gamma) = x \exp(i\beta) - y \exp(i\eta) \tag{28}$$

Note that x, β, $|BI|$ and $|HJ|$ are constant and do not change over time, and $\eta = \theta - \pi/2$. It follows from the real and imaginary parts of Eq. 28 that

$$\gamma = \tan^{-1}\left(\frac{x\sin(\beta) - y\sin(\eta)}{x\cos(\beta) - y\cos(\eta)}\right) \quad \text{and} \quad z = \frac{x\cos(\beta) - y\cos(\eta)}{\cos(\gamma)}$$

Thus analytical expressions for the shock absorber loop's generalized coordinates are thus

$$\angle DBJ = \gamma - \eta \quad \text{and} \quad r = z - (|BI| + |HJ|)$$

For velocity kinematics, time differentiating Eq. 28 leads to

$$0 = i\dot\eta y \exp(i\eta) + i\dot\gamma z \exp(i\gamma) + \gamma \dot z \exp(i\gamma) \tag{29}$$

Multiplying both sides by $\exp(-i\gamma)$ leads to

$$0 = i\dot\eta y \exp(i(\eta - \gamma)) + i\dot\gamma z + \dot z$$

Equating the real and imaginary parts results in

$$0 = -\dot\eta y \sin(\eta - \gamma) + \dot z \quad \Rightarrow \quad \dot z = y\sin(\eta - \gamma)\dot\eta$$

$$\text{and} \quad 0 = \dot\eta y \cos(\eta - \gamma) + \dot\gamma z \quad \Rightarrow \quad \dot\gamma = -\frac{y\cos(\eta - \gamma)}{z}\dot\eta$$

Since $\dot\eta = \dot\theta$ and $\dot r = \dot z$, the expressions for the generalized velocities for the shock absorber loop are

$$\angle\dot{DBJ} = -\left(1 + \frac{y\cos(\eta - \gamma)}{z}\right)\dot\theta$$
$$\dot r = y\sin(\eta - \gamma)\dot\theta$$

The contributions to $X_{\mathfrak{S}}$ are:

$$X_{\mathfrak{S}} = \begin{bmatrix} -\left(1 + \dfrac{y\cos(\eta - \gamma)}{z}\right) \\ y\sin(\eta - \gamma)/r \end{bmatrix} \tag{30}$$

5.3. Spindle/tierod loop kinematics

We use α to denote the 1 degree of freedom generalized coordinate for the spindle's rotation about the DF upright arm. The $\mathfrak{R}(\alpha)$ rotation matrix associated with this generalized coordinate has the form

$$\mathfrak{R}(\alpha) = \begin{pmatrix} \cos(\alpha) & -\sin(\alpha) & 0 \\ \sin(\alpha) & \cos(\alpha) & 0 \\ 0 & 0 & 1 \end{pmatrix} \tag{31}$$

The tierod has 2 degree of freedom generalized coordinates for rotations about the X and Z successive axes at K. We denote these coordinate angles as χ and ζ respectively. The forward kinematics for the spindle/tierod look requires solving for α, χ and ζ as a function of the θ independent generalized coordinate. We have

$$\overrightarrow{EL} - \overrightarrow{EK} = \overrightarrow{KL}$$

Given a value for the independent coordinate θ, the location of O is known, and thus so is the vector $\overrightarrow{EL}$. Thus

$$|\overrightarrow{EL}|^2 + |\overrightarrow{EK}|^2 - 2(\overrightarrow{EL}^*)(\overrightarrow{EK}) = |\overrightarrow{KL}|^2$$

Also $\overrightarrow{EK} = \mathfrak{R}(\alpha)\overrightarrow{EK}_0$, where $\overrightarrow{EK}_0$ is the vector for the unrotated spindle arm. Thus

$$\overrightarrow{EL}^* \mathfrak{R}(\alpha)\overrightarrow{EK}_0 = \frac{1}{2}\left(|\overrightarrow{EL}|^2 + |\overrightarrow{EK}|^2 - |\overrightarrow{KL}|^2\right)$$

Let the elements of the vectors $\overrightarrow{EL}$ and $\overrightarrow{EK}_0$ in the vertical arm frame be given by

$$\overrightarrow{EL} = \begin{bmatrix} \overrightarrow{EL}(x) \\ \overrightarrow{EL}(y) \\ \overrightarrow{EL}(z) \end{bmatrix} \quad \text{and} \quad \overrightarrow{EK}_0 = \begin{bmatrix} \overrightarrow{EK}_0(x) \\ \overrightarrow{EK}_0(y) \\ \overrightarrow{EK}_0(z) \end{bmatrix}$$

With

$$A \triangleq \overrightarrow{EL}(x)\overrightarrow{EK}_0(x) + \overrightarrow{EL}(y)\overrightarrow{EK}_0(y)$$
$$\text{and} \quad B \triangleq -\overrightarrow{EL}(x)\overrightarrow{EK}_0(y) + \overrightarrow{EL}(y)\overrightarrow{EK}_0(x)$$

Eq. 31 leads to

$$A\cos(\alpha) + B\sin(\alpha) = X$$
$$\text{where} \quad X \triangleq \frac{1}{2}\left(|\overrightarrow{EL}|^2 + |\overrightarrow{EK}|^2 - |\overrightarrow{KL}|^2\right) - \overrightarrow{EK}(z)\overrightarrow{EK}_0(z)$$

Defining

$$\beta \triangleq \tan^{-1}\left(\frac{B}{A}\right)$$

we have

$$\cos(\alpha - \beta) = \frac{X}{\sqrt{A^2 + B^2}} \quad \Rightarrow \quad \alpha = \beta \pm \cos^{-1}\left(\frac{X}{\sqrt{A^2 + B^2}}\right)$$

Once α value is determined, the location of the tierod axes at K is known and so is the vector $\overrightarrow{KL}$. The χ and ζ tierod generalized coordinates are then simply the elevation and azimuth angles for the $\overrightarrow{KL}$ vector as seen from the spindle's frame. Using the elements of $\overrightarrow{KL}$ in the spindle fixed frame we then have

$$\chi = \sin^{-1}\left(\frac{\overrightarrow{KL}(z)}{|\overrightarrow{KL}|}\right) \quad \text{and} \quad \zeta = \tan^{-1}\left(\frac{\overrightarrow{KL}(y)}{\overrightarrow{KL}(x)}\right)$$

For velocity kinematics, we need to solve for the $\dot{\alpha}$, $\dot{\chi}$ and $\dot{\zeta}$ generalized velocities for the spindle loop as a function of the $\dot{\theta}$ independent generalized velocity. For a given, $\dot{\theta}$, we can use the analytical velocity expressions derived so far in this expression to compute the v_E linear velocity of point E on the spindle with respect to A on the chassis. Since the end of the tierod L is constrained by a ball joint to the chassis, the relative motion from the spindle loop generalized velocities when combined with v_E has to result in zero linear velocity at L. Thus

$$v_E + \mathcal{J}_{EL}\begin{bmatrix}\dot{\alpha}\\\dot{\chi}\\\dot{\zeta}\end{bmatrix} = 0 \quad \Rightarrow \quad \begin{bmatrix}\dot{\alpha}\\\dot{\chi}\\\dot{\zeta}\end{bmatrix} = -\mathcal{J}_{EL}^{-1}v_E$$

where $\mathcal{J}_{EL}$ denotes the 3×3 Jacobian that maps the spindle generalized velocities into the linear velocity of L with respect to E on the spindle. The columns of this Jacobian are simply the cross product of the vector from the spindle hinge axis location to L and the hinge axis for each of the three hinge axes. Additionally, with $\mathcal{J}_{AE}$ and $\mathcal{J}_{DE}$ denoting the 3×1 Jacobian matrices for the v_E linear velocity from the A and D hinge degrees of freedom, we have

$$v_E = [\mathcal{J}_{AE}, \mathcal{J}_{DE}]\begin{bmatrix}\dot{\theta}\\\angle\dot{NDO}\end{bmatrix} \overset{27}{=} [\mathcal{J}_{AE} + (p-1)\mathcal{J}_{DE}]\dot{\theta}$$

$$\Rightarrow \quad \begin{bmatrix}\dot{\alpha}\\\dot{\chi}\\\dot{\zeta}\end{bmatrix} = -\mathcal{J}_{EL}^{-1}[\mathcal{J}_{AE} + (p-1)\mathcal{J}_{DE}]\dot{\theta} \tag{32}$$

Eq. 32 defines the contribution of the spindle loop to the $X_\mathbb{G}$ matrix for the velocity kinematics.

5.4. Front steering kinematics

Figure 6 shows a schematic for the Pitman steering mechanism for the front wheels. With T and W being points on the chassis, the TU and WV links are the left and right idler arms respectively that connect to the $LUVL$ steering link. The L end points of the steering link are connected to the tierods for the front wheels. $TUVW$ represents a planar four-bar loop within the mechanism. Steering changes the $\angle XTU$ angle causing the steering link, and consequently the left and right wheel tierods to move and change the orientation of the front wheels. For the purposes of dynamics modeling, the only contribution of the
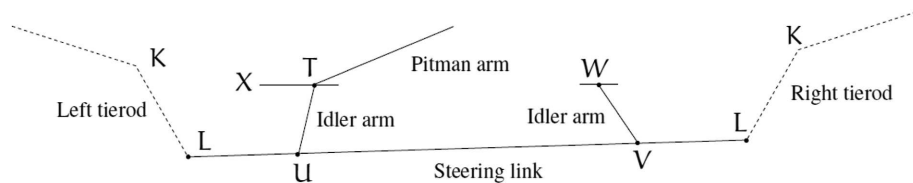

Fig. 6. Schematic for the Pitman steering mechanism for the front wheels

steering mechanism is to the positioning of the tierod end points for the front wheels. The analytical approach for four-bar mechanism forward kinematics used in Section 5.1 can be used for the Pitman steering to determine its shape as a function of the steering angle and consequently the location of the tierod end points. The instantaneous location of the tierod endpoints are used in the spindle kinematics described in Section 5.3 for the front suspensions.

6. Conclusions

In this paper we describe in detail the application of constrained embedding technique for the modeling of the dynamics of a HMMWV vehicle with double wishbone suspension systems. Constraint embedding allows us to formulate the dynamics as an ODE system, and in a way that preserves the underlying structure of the system so that low-cost recursive methods for minimal coordinate systems can be applied for solving the equations of motion. We further illustrate analytical kinematic techniques for the HMMWV double wishbone suspension that can be used to speed up and improve the accuracy of the overall vehicle dynamics.

Acknowledgments

The research described in this paper was performed at the Jet Propulsion Laboratory (JPL), California Institute of Technology under contract with the National Aeronautics and Space Administration, and at the U.S. Army TARDEC.* Cleared for public release.

REFERENCES

[1] Haug E. J.: Elements of Computer-Aided Kinematics and Dynamics of Mechanical Systems: Basic Methods. Springer-Verlag, 1984.

[2] Abhinandan Jain: Multibody graph transformations and analysis Part II: Closed-chain constraint embedding. Nonlinear Dynamics, 67(3):2153-2170, August 2012.

[3] Abhinandan Jain: Robot and Multibody Dynamics: Analysis and Algorithms. Springer, 2011.

[4] Reinhold von Schwerin: Multibody system simulation: numerical methods, algorithms, and software. Springer, 1999.

[5] Paramsothy Jayakumar, Abhinandan Jain, James Poplawski, Marco B Quadrelli, and Jonathan M Cameron: Advanced Mobility Testbed for Dynamic Semi-Autonomous Unmanned Ground Vehicles. In NATO Meeting AVT-241/RSM-022: Technological and Operational Problems Connected with UGV Application for Future Military Operations, Rzeszow, Poland, 2015.

[6] Jonathan M Cameron, Steven Myint, Calvin Kuo, Abhinandan Jain, Havard F Grip, Paramsothy Jayakumar, and Jim Overholt: Real-Time and High-Fidelity Simulation Environment for Autonomous Ground Vehicle Dynamics. In 2013 NDIA Ground Vehicle Systems Engineering and Technology Symposium, Troy, Michigan, 2013.

[7] Abhinandan Jain, Calvin Kuo, Paramsothy Jayakumar, and Jonathan M Cameron: A Constraint Embedding Approach for Complex Vehicle Suspension Dynamics. In ECCOMAS Thematic Conference on Multibody Dynamics, Barcelona, Spain, 2015.

[8] Guillermo Rodriguez, Abhinandan Jain, and K Kreutz-Delgado: A spatial operator algebra for manipulator modeling and control. INTRR, 10(4):371, 1991.

[9] Abhinandan Jain, Cory Crean, Calvin Kuo, and Marco B Quadrelli: Efficient Constraint Modeling for Closed-Chain Dynamics. In The 2nd Joint International Conference on Multibody System Dynamics, Stuttgart, Germany, 2012.

[10] Randy Sleight: Modeling and Control of an Autonomous HMMWV. PhD thesis, University of Delaware, 2004.

[11] Justin Madsen: A Stochastic Framework for Ground Vehicle Simulation. PhD thesis, University of Wisconsin, Madison, 2009.

Metoda więzów wbudowanych w modelowaniu dynamiki zawieszenia pojazdu

S t r e s z c z e n i e

Celem badań było uzyskanie osiągów bliskich dynamice czasu rzeczywistego, by umożliwić testowanie bezzałogowych pojazdów naziemnych (UGV) z autopilotem w zamkniętej pętli w wa-

---

runkach ruchu miejskiego i jazdy terenowej. O ogólnych osiągach dynamicznych pojazdu decyduje model dynamiczny układu wielu ciał dla tego pojazdu, dynamika oddziaływań wzajemnych kół i podłoża i pokładowy system sterowania. Tematem artykułu jest opracowanie wydajnego obliczeniowo i dokładnego modelu dynamiki pojazdu naziemnego ze złożoną dynamiką zawieszenia. Wyzwanie polega na tym, że typowe zawieszenia pojazdów zawierają pętle łańcuchów zamkniętych, które wymagają kosztownych technik całkowania równań różniczkowo-algebraicznych (DAE). W artykule autorzy zilustrowali zastosowanie podejścia alternatywnego, metody więzów wbudowanych (*Constraint Embedding*, CE), co pozwala zredukować koszty obliczeniowe i poprawić dokładność modelu dynamiki pojazdu.